Rees, D.; Groth, M.; Aleiferis, S.; Brezinsek, S.; Brix, M.; Jepu, I.; Lawson, K. D.; Meigs, A. G.; Menmuir, S.; Kirov, K.; Lomas, P.; Lowry, C.; Thomas, B.; Widdowson, A.; Carvalho, P.; Delabie, E.; JET Contributors

Characterisation of the scrape-off layer in JET-ILW deuterium and helium low-confinement mode plasmas

Published in:
Nuclear Materials and Energy

DOI:
10.1016/j.nme.2024.101657

Published: 01/06/2024

Document Version
Publisher's PDF, also known as Version of record

Nuclear Materials and Energy 39 (2024) 101657

Contents lists available at ScienceDirect

Nuclear Materials and Energy

journal homepage: www.elsevier.com/locate/nme

Characterisation of the scrape-off layer in JET-ILW deuterium and helium low-confinement mode plasmas

D. Rees [a,*], M. Groth [a], S. Aleiferis [b], S. Brezinsek [c], M. Brix [b], I. Jepu [b], K.D. Lawson [b], A.G. Meigs [b], S. Menmuir [b], K. Kirov [b], P. Lomas [b], C. Lowry [b], B. Thomas [b], A. Widdowson [b], P. Carvalho [b], E. Delabie [d], JET Contributors[1]

[a] Aalto University, Department of Applied Physics, Espoo, Finland
[b] UKAEA, Culham Science Centre, Abingdon, UK
[c] Forschungszentrum Jülich GmbH, Institute for Energy and Climate Research Plasma Physics, Jülich, Germany
[d] Oak Ridge National Laboratory, Oak Ridge, 37831-6304, TN, USA

ARTICLE INFO

Keywords:
Helium plasma
Detachment
JET
Tokamak
Divertor
SOL

ABSTRACT

Langmuir probe measurements in neutral beam injection (NBI) heated, low-confinement mode plasmas in JET ITER-like wall showed that the current to the divertor targets, I_{div}, in helium (He) plasmas was up to 70 % lower on the low-field side (LFS) than in otherwise identical deuterium (D) plasmas. The edge plasma density at which the rollover of I_{div} occurred i.e. the onset of detachment, was 10 % higher in He plasmas on both the LFS and high-field side (HFS). The density of I_{div} rollover increases by 25 % for He when the NBI power increases 1 MW to 5 MW. The total radiated power was similar in He and D plasmas for densities below the I_{div} rollover. At densities above the I_{div} rollover density, the total radiated power and power from within the separatrix are higher in He, reducing the power across the separatrix and subsequently $I_{div,LFS}$. In He plasmas, the peak radiated power was observed within the confined region above the X-point in tomographic reconstructions from bolometry.

1. Introduction

The ITER Pre-fusion Power Operation phase foresees experiments in hydrogen and helium (He) plasmas to demonstrate plasma operation in low-confinement mode (L-mode) [1]. ITER – and future power-producing reactors – require divertor detachment to reduce the heat flux onto the divertor target to powers $<20\,MW\,m^{-2}$ [2–4]. Experiments for the study of the scrape-off layer (SOL) and detachment in plasmas with He as the main ion species have previously been performed in JET with an all-carbon wall, JET-C [5,6], the carbon-walled DIII-D [7], and the water-cooled tungsten divertor tokamak EAST [8]. This paper presents experiments with He and deuterium (D) plasmas performed in JET ITER-like wall (JET-ILW), which has beryllium wall tiles and a tungsten divertor [9].

It is necessary to simulate detachment for the planning of operating current reactors and the design of future reactors. Current edge plasma simulations for hydrogenic plasmas do not quantitatively reproduce all experimental observations. In hydrogenic simulations, divertor current at the onset of detachment and the radiated power is under-predicted by a factor of 2 by the 2D edge fluid codes SOLPS-ITER and EDGE2D-EIRENE [10,11]. Mass rescaling of molecular charge exchange rates changes the divertor neutral density by 100% [12]. Helium plasmas offer a way to validate codes and SOL physics understanding through comparison with the more typical D plasmas. He has the highest first ionisation energy, longer mean-free-path of ionisation, and lacks molecules.

2. Experimental setup

Experiments with ^{4}He and D neutral beam injection (NBI) heated L-mode plasmas were conducted in JET-ILW with JET-typical machine parameters of $\vec{B}\times\nabla B$ towards the divertor, an on-axis toroidal field, B_T, of 2.5 T, a plasma current, I_p, of 2.4 MA, and an edge safety factor, q_{95}, of 3.2. The experiments were conducted in a vertical–horizontal divertor configuration – optimised for diagnostics and edge modelling [13] – where the high-field side (HFS) strike point is on the HFS vertical plate and the low-field side (LFS) strike point is on the horizontal plate (Fig. 1). Fuelling was performed through gas injection to the HFS

* Corresponding author.
E-mail address: david.rees@aalto.fi (D. Rees).
[1] See the author list of: 'Overview of JET results for optimising ITER operation' J. Mailloux et al. 2022, Nucl. Fusion 62, 042026

https://doi.org/10.1016/j.nme.2024.101657
Received 6 August 2023; Received in revised form 25 March 2024; Accepted 17 April 2024
Available online 20 April 2024

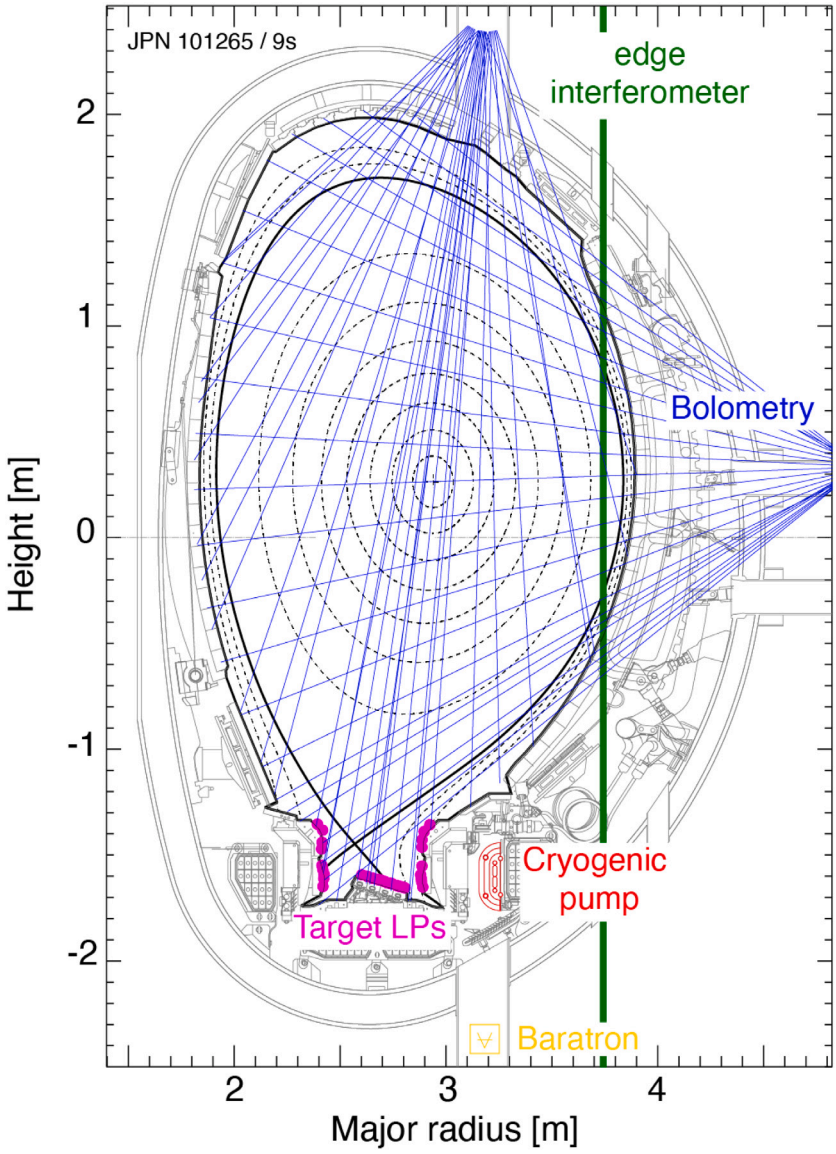

Fig. 1. Schematic of the JET vessel structure (grey) and magnetic equilibrium (black) for the He pulse JPN 101265 with relevant components shown, the cryogenic pump (red), target Langmuir probes (magenta), far-infrared interferometer (green), vertical and horizontal bolometry lines of sight (blue), and baratron pressure gauge (yellow). (For interpretation of the references to colour in this figure legend, the reader is referred to the web version of this article.)

divertor either continuously, for fuelling ramps, or intermittently to hold the plasma at set densities, for fuelling steps. NBI heating was applied with the same species as the plasma main ion, at $P_{\mathrm{NBI}} = 1\,\mathrm{MW}$ in D and 1 MW, 2 MW, and 5 MW in He. The highest total heating power, P_{T}, was 3.5 MW and 7 MW for D and He, respectively. Higher P_T in L-mode confinement were permissible in the He plasmas due to the higher L-H transition power threshold in He [14]. The purity across all He pulses was $c_{\mathrm{He}} = n_{\mathrm{He}}/n_{\mathrm{e}} = (49.5 \pm 0.2)\%$, as measured by the sub-divertor optical Penning gauge [15]. The experimental setup, characterisation, and modelling efforts of the D plasmas have been previously described in Refs. [10,13,16–20].

The He experiments utilised argon frosting of the divertor cryogenic panel for improve density control but the pumping rate in these plasmas is unknown. A study of Ar-frosting in the MkII-GB configuration of JET found a maximum pumping rate for He of $95\,\mathrm{m^3\,s^{-1}}$. The pumping rate was not constant through the pulse and dropped to as low as $20\,\mathrm{m^3\,s^{-1}}$. The pumping rate for D_2 was $125\,\mathrm{m^3\,s^{-1}}$ [21]. Thus the He pumping performance in this works plasmas is also likely poor.

Sweeps of the strike points over the divertor targets were conducted to produce continuous profiles of the ion saturation current density, j_{sat}, electron temperature, T_e, and electron density, n_e, measured by the divertor Langmuir probes (LPs, Fig. 1). Integration over the j_{sat} profile provided the total ion current to the target plates, I_{div}. The LP measurements of n_e have an ion mass and charge dependence, and require an assumption of the charge state of impinging ions. The effective charge was assumed to be $Z_{\mathrm{eff}} = 1$ and 1.5 for D and He, respectively. For D plasmas, I_{div} is directly proportional to the ion flux $\Gamma_{\mathrm{div}}^{\mathrm{D+}}$ but for He plasmas, total He ion flux is between $0.5{-}1 \times \Gamma_{\mathrm{div}}^{\mathrm{D+}}$ depending on the ratio of He^{+2} to He+ impinging the targets. The peak plasma pressure at the target was estimated from the LPs n_e and T_e profiles by $p_{\mathrm{total}} = p_{\mathrm{dynamic}} + p_{\mathrm{static}} = m_i Z_{\mathrm{eff}}^{-1} n_e c_s^2 + (Z_{\mathrm{eff}}^{-1} + 1) n_e k_B T_e$, where $T_i = T_e$ is assumed.

The total gas pressure in the sub-divertor was measured using a capacitance manometer (baratron) located below the cryogenic pump [22,23]. Baratrons are gas-species independent, such that the measured pressure is of molecular D_2 and atomic He.

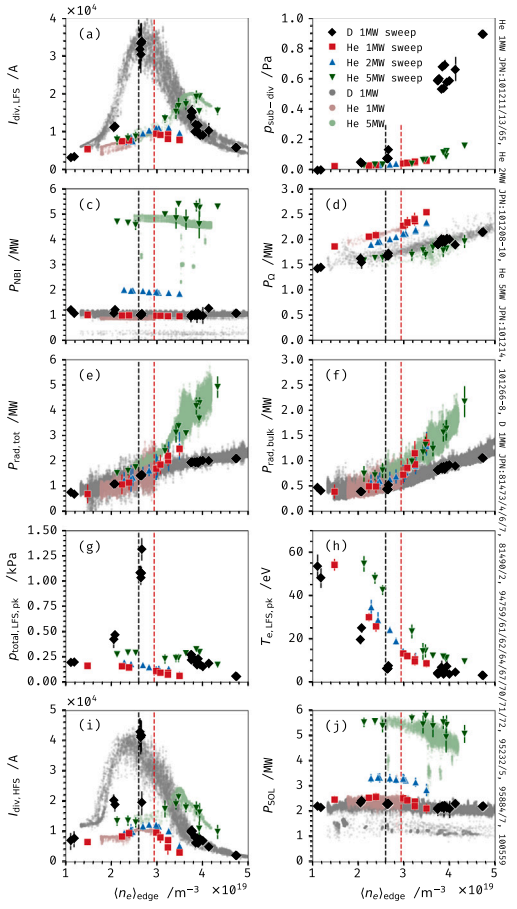

Fig. 2. (a) LFS divertor ion current from integration over the LPs, (b) baratron sub-divertor neutral pressure, (c) NBI heating power, (d) Ohmic heating power, (e) total radiated power measured by bolometry, (f) radiated power from within the region confined by the separatrix, (g) peak estimated pressure on the LFS target, (h) peak electron temperature on the LFS target, (i) HFS divertor ion current, and (j) power crossing the separatrix into the SOL as a function of LFS edge line-averaged electron density. The legend in (b) applies to all sub-plots. The He pulses with P_{NBI} = 1 MW of heating and strike point sweeps (JPN 101211/3) are marked with red squares, the 1 MW He density ramp (JPN 101265) with pale red circles, 2 MW He sweeps (JPN 101208-10) with blue up triangles, 5 MW He sweeps (JPN 101214, 101267/8) with green down triangles, 5 MW He ramp (JPN 101266) with pale green circles, 1 MW D sweeps (JPN 81473/4/6/7, 81490/2, 94767, 94770-72, 95884/7) with grey circles, and 1 MW D ramps (JPN 94759/61/62/64, 95232/35, 100559) with black diamonds. The detachment onset density is indicated with vertical dashed lines in black and red for 1 MW D and 1 MW He, respectively. (For interpretation of the references to colour in this figure legend, the reader is referred to the web version of this article.)

The radiated power was measured by the JET bolometry system [24]. The lines-of-sight of the vertical and horizontal cameras are shown in Fig. 1. Tomographic reconstructions from the two bolometers provided 2D profiles of the radiated power.

The LFS edge line-averaged electron density, $\langle n_e \rangle_{edge}$, measured by the far-infrared interferometer [25] in Fig. 1, was used as a proxy for the SOL upstream electron density and as the primary independent parameter.

3. Results and discussion

The D plasmas showed the expected rollover behaviour of $I_{div,LFS}$ against $\langle n_e \rangle_{edge}$ with no difference observed between fuelling ramps and steps (Fig. 2a). The peak of I_{div} rollover against $\langle n_e \rangle_{edge}$ is considered here to be the detachment onset density, as used in previous studies [5,8,19]. $I_{div,LFS}$ and $I_{div,HFS}$ were fit for each pulse with Gaussian process regression [26] to find the average LFS rollover edge density in P_{NBI} = 1 MW He $n_{e,det,He} = (2.94 \pm 0.09) \times 10^{19}$ m^{-3} and in D $n_{e,det,D} = (2.6 \pm 0.1) \times 10^{19}$ m^{-3}. The HFS rollover occurred at ~10% lower edge density than the LFS in both species (Fig. 2i). For P_{NBI} = 1 MW in He, $n_{e,det,HFS,He} = (2.60 \pm 0.04) \times 10^{19}$ m^{-3} and for D, $n_{e,det,HFS,D} = (2.3 \pm 0.1) \times 10^{19}$ m^{-3}. Detachment of the HFS at lower upstream densities than the LFS is typical behaviour in tokamaks when the $\vec{B} \times \nabla B$ drift is towards the divertor, as $\vec{E} \times \vec{B}$ drifts drive a flow of particles from the LFS divertor into the PFR and from the PFR into the HFS divertor [27]. In JET-C, rollover of $I_{div,LFS}$ occurred at ~30% higher $\langle n_e \rangle_{edge}$ in He than D [5].

Ohmic heating power, P_Ω, was 30% higher in He than D P_{NBI} = 1 MW plasmas (Fig. 2d) due to the higher Spitzer resistivity of the higher Z_{eff} of the He^{2+} core plasma. The radiation from the confined region as measured by bolometry, $P_{rad,bulk}$, and total radiated power, $P_{rad,tot}$, was the same within measurement uncertainty between P_{NBI} = 1 MW He and D for $\langle n_e \rangle_{edge} < n_{e,det,He}$ (Fig. 2e and f). The power across the separatrix was estimated by $P_{SOL} = P_\Omega + P_{NBI} - P_{rad,bulk}$ (Fig. 2j). For $\langle n_e \rangle_{edge} < n_{e,det,He}$, P_{SOL} was 10% higher in He than D, due to the higher P_Ω in He plasmas, which contributes to the observed higher I_{div} rollover density in He. In D plasmas, $P_{rad,bulk}$ and $P_{rad,tot}$ are proportional to P_Ω with increasing $\langle n_e \rangle_{edge}$ and show no relationship to I_{div} rollover. The continued increase of radiated power with increasing $\langle n_e \rangle_{edge}$ is a defining feature of detachment [28]. In He however, for $\langle n_e \rangle_{edge} > n_{e,det,He}$, $P_{rad,bulk}$ and $P_{rad,tot}$ increase at a greater rate than P_Ω with increasing $\langle n_e \rangle_{edge}$. The increase in $P_{rad,bulk}$ reduces P_{SOL} by ~15%, to the same as in the D plasmas.

The sub-divertor neutral pressure was observed to be independent of heating power in the He plasma (Fig. 2b). The higher pressure observed in D than He is likely due to the higher recycling at the targets, but the sub-divertor pressure was found to be unsuitable as a proxy for the target neutral pressure as it is governed by the throughput of the pumping plena and the pumping speed of the cryogenic pump, which is different for the two species [29].

In He plasmas with P_{NBI} = 1 MW of NBI heating, $I_{div,LFS}$ was up-to four times lower than in P_{NBI} = 1 MW D (Fig. 2a). Currently, the cause of the difference is unclear, and is likely caused by a combination of factors. One factor is the effective electron cooling (or 'ionisation cost'), E_{ion}, associated with the ionisation of the recycling neutrals by the SOL plasma, which is higher for He than D for $T_e \gtrsim 10$ eV. The ion current to the divertor in high-recycling conditions is approximately described by,

$$I_{div} = \frac{P_{SOL} - P_{rad,imp}}{E_{ion}} - S_{rec} \quad (1)$$

where $P_{rad,imp}$ is the impurity radiated power, S_{rec} is the recombination rate and plasma [30,31]. As $P_{rad,bulk}$ was the same between the two species for $\langle n_e \rangle_{edge} < n_{e,det,He}$, for Eq. (1) $P_{rad,imp}$ is assumed to also be the same in both species. As P_{SOL} was observed to be 10% higher in He than D. In high-recycling conditions ($T_e \sim 30$ eV, $n_e = 2 \times 10^{19}$ m^{-3}) $E_{ion,He} \approx 35$ eV for He^0 ionisation and $E_{ion,D} \approx 24$ eV for D^0 ionisation [32], which produces a 25% reduction from I_{div} with D to I_{div} with He. An additional energy loss to the ionisation of the singly charged ion, $e + He^{+1} \longrightarrow He^{+2} + 2e$, will further reduce ion current. However, the distribution of charge states of He in the divertor is unknown and AMJUEL currently does not include E_{ion} for the reaction. The charge exchange rate is ~ 10× lower for He than D and may also contribute to the lower ion current. Simulations of the He plasmas with SOLPS-ITER is expected to allow analysis of quantities that cannot be experimentally measured and determine the contributions to the lower recycling in He compared with D plasmas.

The $\langle n_e \rangle_{edge}$ of I_{div} rollover scales with NBI power; increasing heating in He from P_{NBI} = 1 MW to 2 MW (Fig. 2 blue up triangles) increases $n_{e,det,He}$ by 10% and from 1 MW to 5 MW (Fig. 2 green down triangles) by 25%. In He P_{NBI} = 5 MW plasmas, $p_{total,LFS,pk}$ and $T_{e,LFS,pk}$ do not reduce to match measurements in He P_{NBI} = 1 MW plasmas at $\langle n_e \rangle_{edge} > n_{e,det,He,5\ MW}$. The effect of higher core temperature lowering resistivity

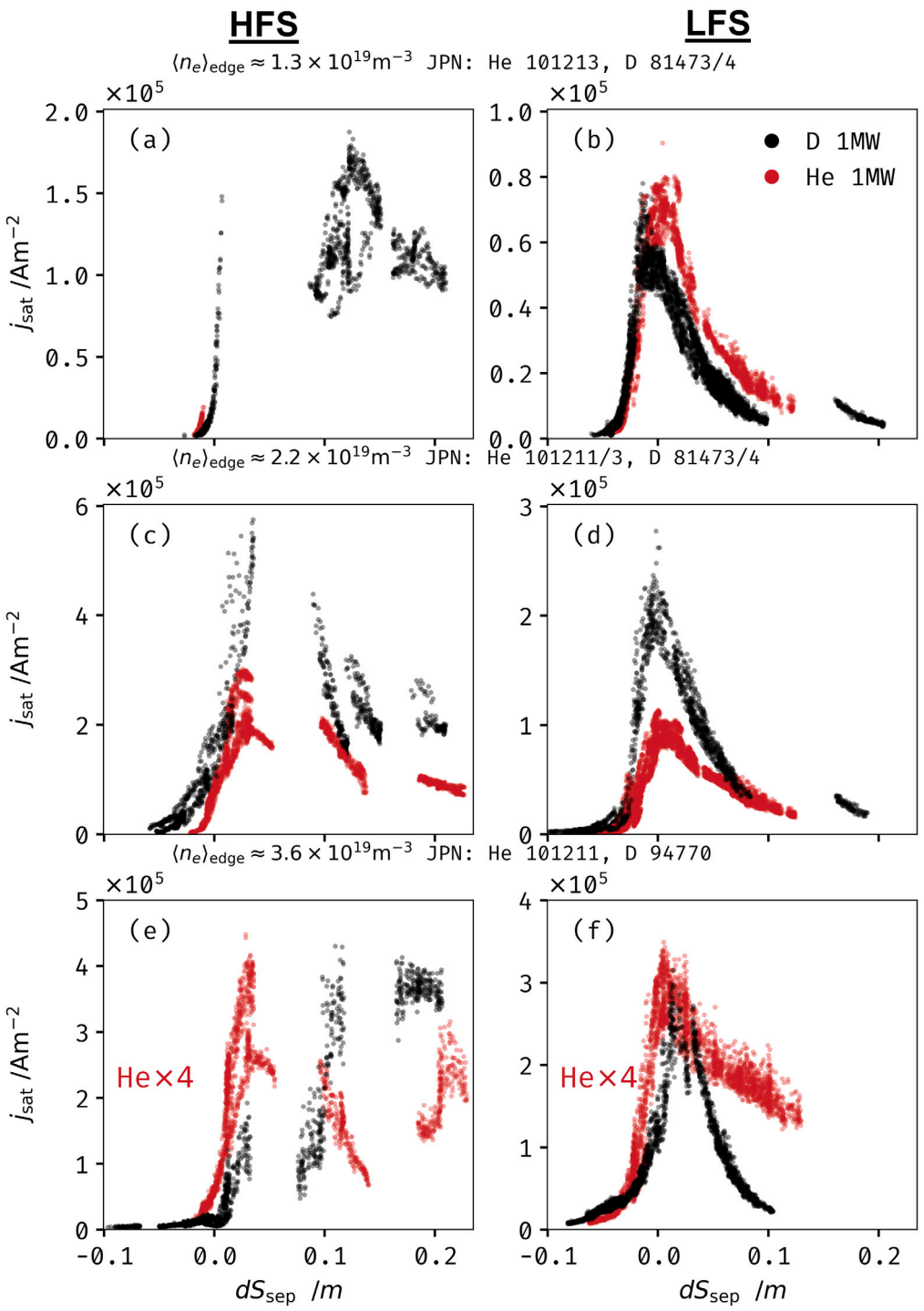

Fig. 3. Divertor target profiles for P_{NBI} = 1 MW of the He (red) and D (black) ion saturation current density from the Langmuir probes on the high-field side (a, c, e) and low-field side (b, d, f). The top row (a, b) shows low-density sweeps ($\langle n_e \rangle_{edge} \approx 1.3 \times 10^{19}$ m^{-3}, He JPN 101213, D JPN 81473/4), the middle row (c, d) shows mid-density sweeps (2.2×10^{19} m^{-3}, He JPN 101211/3, D JPN 81473/4), and the bottom row (e, f) shows high-density sweeps (3.6×10^{19} m^{-3}, He JPN 101211, D JPN 94770). The He signal is scaled by ×4 in (e) and (f) for readability. (For interpretation of the references to colour in this figure legend, the reader is referred to the web version of this article.)

was observed in the P_{NBI} = 2 MW and 5 MW He pulses, which had 7% and 25% lower P_{Ω} than 1 MW He, respectively.

The peak $j_{sat,LFS}$ in He was found to be insensitive to $\langle n_e \rangle_{edge}$, increasing by ~30% from low-density to mid-density compared to ~90% in D (Fig. 3b and d). The He $j_{sat,LFS}$ profile was broader than in D. It is difficult to determine the peak $j_{sat,HFS}$ due to a gap in the LPs that obscures wherever the strike point has been observed, however the current to the HFS target was generally higher than the LFS for both species (Fig. 3a, c, and e).

In P_{NBI} = 1 MW plasmas at low-density, He and D both have a peak $T_{e,LFS}$ of ~60 eV and at mid-density, $\langle n_e \rangle_{edge} \approx 2.2 \times 10^{19}$ m^{-3}, the peak deceases to ~30 eV, Fig. 4b and d, respectively. The same broader profile for He observed in j_{sat} is also apparent in T_e. At high-density, $\langle n_e \rangle_{edge} \approx 3.6 \times 10^{19}$ m^{-3}, the peak $T_{e,LFS}$ measured by the LPs

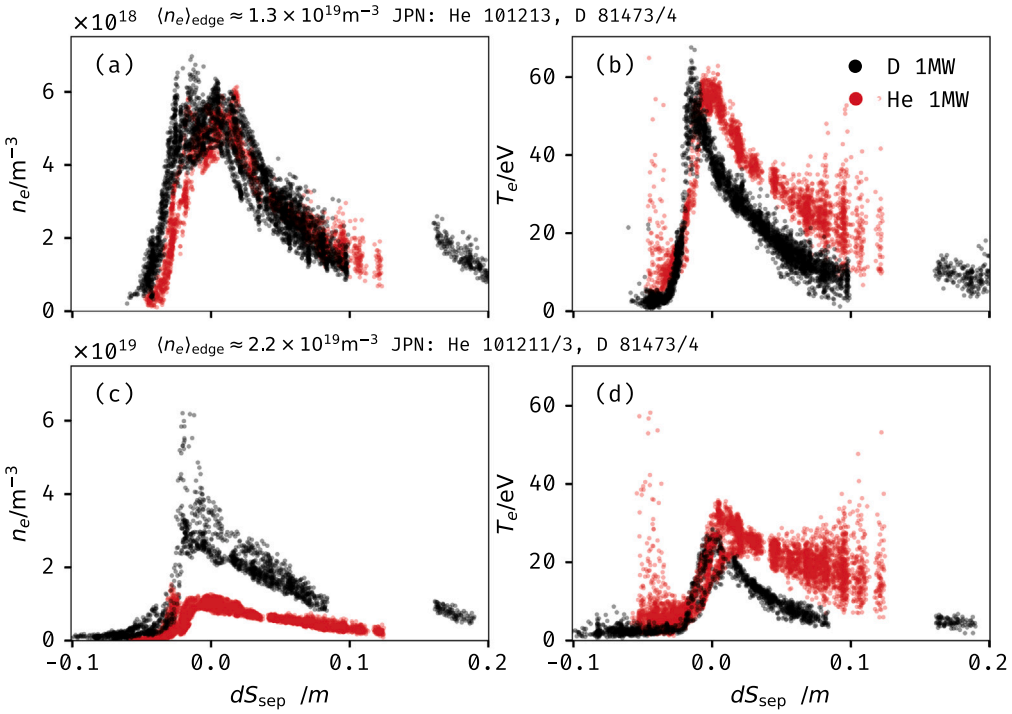

Fig. 4. Low-field side divertor target profiles for $P_{NBI} = 1$ MW of the He (red) and D (black) electron density (a, c) and electron temperature (b, d) from the Langmuir probes. On the top row (a, b) the low-density sweeps are shown, $\langle n_e \rangle_{edge} \approx 1.3 \times 10^{19}$ m^{-3}, He JPN 101213, D JPN 81473/4. The bottom row (c, d) shows mid-density sweeps, 2.2×10^{19} m^{-3}, He JPN 101211/3, D JPN 81473/4. High-density is excluded due to unreliability of LPs in those conditions. Note that the scale for electron density is different for the two cases. (For interpretation of the references to colour in this figure legend, the reader is referred to the web version of this article.)

for He was <10 eV and D was <5 eV, but LPs are known to overestimate T_e in high-recycling and detached conditions [33,34]. For two of the $P_{NBI} = 1$ MW D pulses included in this work (JPN 94759 and 94771), T_e was derived from deuterium Balmer line emission, which showed the LFS strike point at $\langle n_e \rangle_{edge} = n_{e,det,D}$ to be $T_{e,LFS} \approx 2.5$ eV and at high-density, $T_{e,LFS} \approx 0.8$ eV [17]. More accurate temperature measurements are not available for the He plasmas but from the D estimate, it is likely that at high-density $T_{e,LFS} \ll 10$ eV but not as low as for D.

The LFS target peak electron density, n_e, at mid-density is a factor of two lower for $P_{NBI} = 1$ MW He plasmas than D plasmas. The lower n_e and similar T_e combine to the low $p_{total,LFS,pk}$ observed for the He plasmas.

The 2D radiated power distribution was dependent on $\langle n_e \rangle_{edge}$ and had similar profiles for the two species at low-density but diverged as density increased. For $P_{NBI} = 1$ MW at low-density, the peak emission was close to the HFS vertical target and, although $P_{rad,tot}$ was the same in both species, D had higher power density, with a peak power of 0.30 MW m^{-3}, whereas He was more distributed, peaking at 0.18 MW m^{-3} (Fig. 5a and b). At mid-density, the peak radiated power in He was observed above the X-point, whereas in D the peak was still on the HFS (Fig. 5c and d).

For $\langle n_e \rangle_{edge} \approx 3.6 \times 10^{19}$ m^{-3} > $n_{e,det,He}$, the total radiated power was higher in He than D. The He peak power density was almost doubled going from $\langle n_e \rangle_{edge} = 2.2 \times 10^{19}$ m^{-3} to 3.6×10^{19} m^{-3} but in D, across a similar density increase, the peak power was unchanged. This coincides with the majority of radiated power in He concentrating to the confined region above the X-point and towards the core along the inside of the separatrix (Fig. 5e), which was also observed with He plasmas in JET-C [5]. For a similar edge density in D plasmas, the LFS divertor was the dominate radiator (Fig. 5f).

In $P_{NBI} = 5$ MW He plasmas the power distribution with $\langle n_e \rangle_{edge}$ scaling behaves similar to the $P_{NBI} = 1$ MW He plasmas (Fig. 6). At low-density the 2D profile was similar to He 1 MW at low-density. At mid-density the peak emission was in the region above the X-point, but with strong emission from the LFS divertor. For $\langle n_e \rangle_{edge} > n_{e,det,He,5\ MW}$ in 5 MW He, radiated power was concentrated above the X-point. The peak power density in the high-density case, Fig. 6c, is 1.5 MW m^{-3}.

In D plasmas the rollover of $I_{div,LFS}$ is accompanied by a similar rollover of the estimated peak LFS target plasma pressure, $p_{total,LFS,pk}$ (Fig. 2g). $p_{total,LFS,pk}$ is reduced in $P_{NBI} = 1$ MW He for $\langle n_e \rangle_{edge} > n_{e,det,He}$ but does not increase and rollover with increasing edge density. The peak electron temperature at the LFS target, $T_{e,LFS,pk}$, decreases with increasing $\langle n_e \rangle_{edge}$ for both species, starting at the lowest upstream density of the experiments, $\langle n_e \rangle_{edge} \approx 1{\times}10^{19}$ m^{-3} (Fig. 2h). The reduction in particle and power flux to the targets without a reduction in the plasma pressure further upstream in the SOL in D plasmas is driven by losses to impurity radiation, volumetric recombination, molecular assisted dissociation (MAD), and ion-neutral momentum loss [28,35,36]. These processes drop $I_{div,LFS}$ to 18% of peak and reduce $T_{e,LFS,pk}$ to <0.8 eV. In He plasmas, the long mean-free-path for He^0 ionisation combined with lower divertor densities pushes the ionisation front to above the X-point as $\langle n_e \rangle_{edge}$ increases and $T_{e,LFS,pk}$ decreases, developing a region of intense radiation above the X-point seen in Fig. 5. With the ionisation front inside the confined region, power is lost to the greater $P_{rad,bulk}$, reducing P_{SOL} and subsequently $I_{div,LFS}$, but not to the extent seen by D detachment, and without reducing $T_{e,LFS,pk}$ to the <5 eV seen in D plasmas.

4. Summary

Experiments in JET-ILW L-mode He and D plasmas showed that He plasmas have lower recycling, lower sub-divertor pressures, low target plasma pressures, 10% higher P_{SOL}, and broader divertor target profiles

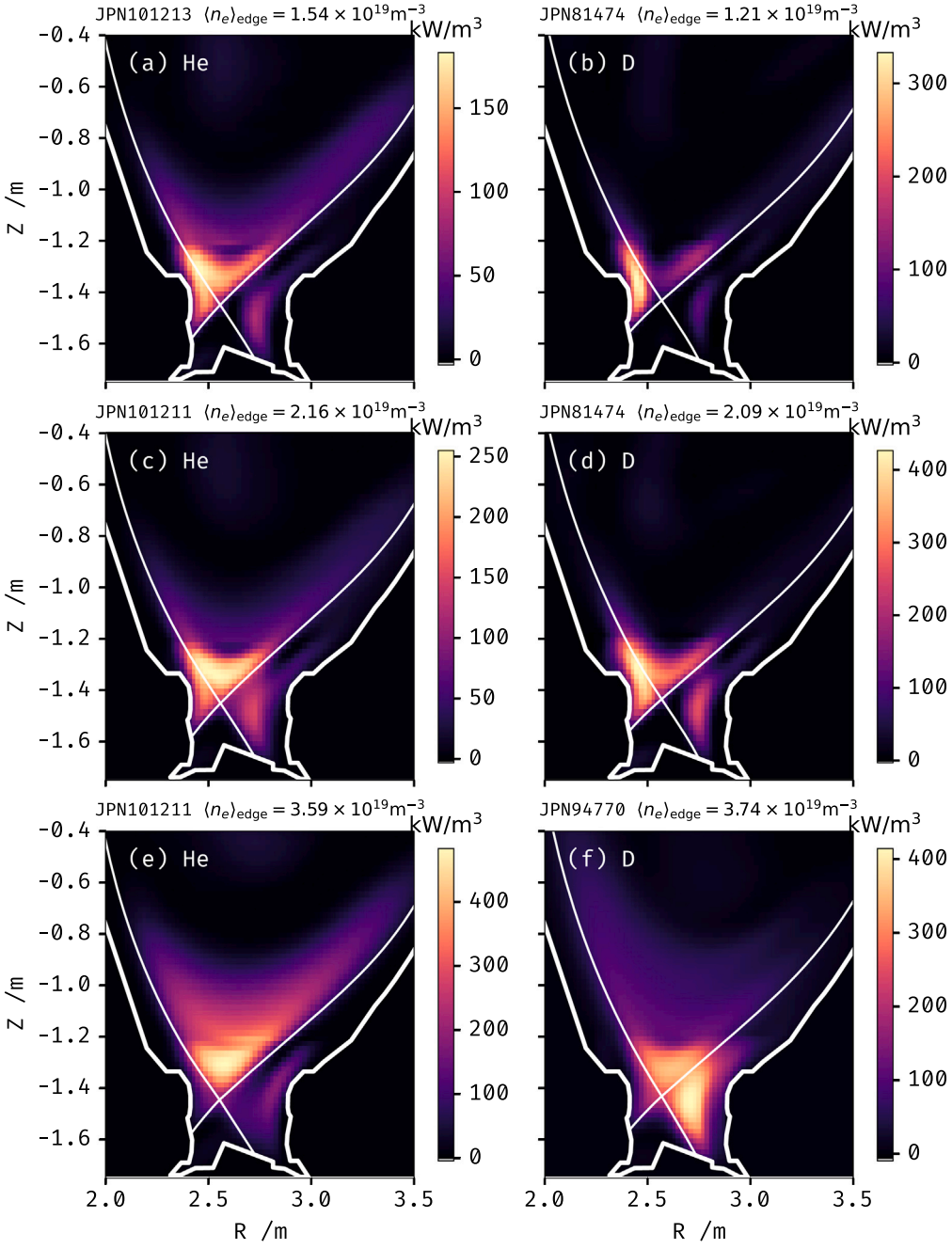

Fig. 5. Total radiated power density tomographic reconstructions from bolometry of P_{NBI} = 1 MW He (a, c, e) and D (b, d, f) plasmas for the low, mid and high-density cases by row.

in j_{sat} and $T_{e,LFS}$. A ~ 10% higher $\langle n_e \rangle_{edge}$ for the onset of detachment was found for He compared with D plasmas, partially due to higher Ohmic heating in He.

In He plasmas with P_{NBI} = 1 MW, $I_{div,LFS}$ in He is up to 70% less than in D. Partially caused by the higher ionisation cost of neutral He compared with D and an unquantified loss to the ionisation of He^+. Additional processes involved in the lower recycling in He plasmas are unknown but simulations of the experiments presented here in future work will elucidate the physics behind this difference.

A concentration of radiated power within the confined region above the X-point, occurring at edge densities less than the detachment threshold, was seen in 2D bolometry reconstructions. In conditions approaching $\langle n_e \rangle_{edge} = n_{e,det,He}$, He atoms recycled at the target can penetrate further through the plasma and into the confined region due to their longer ionisation mean-free path compared to D. Moving the ionisation front to above the X-point increases the power radiated within the confined region, reducing P_{SOL} and thus $I_{div,LFS}$ at the divertor target.

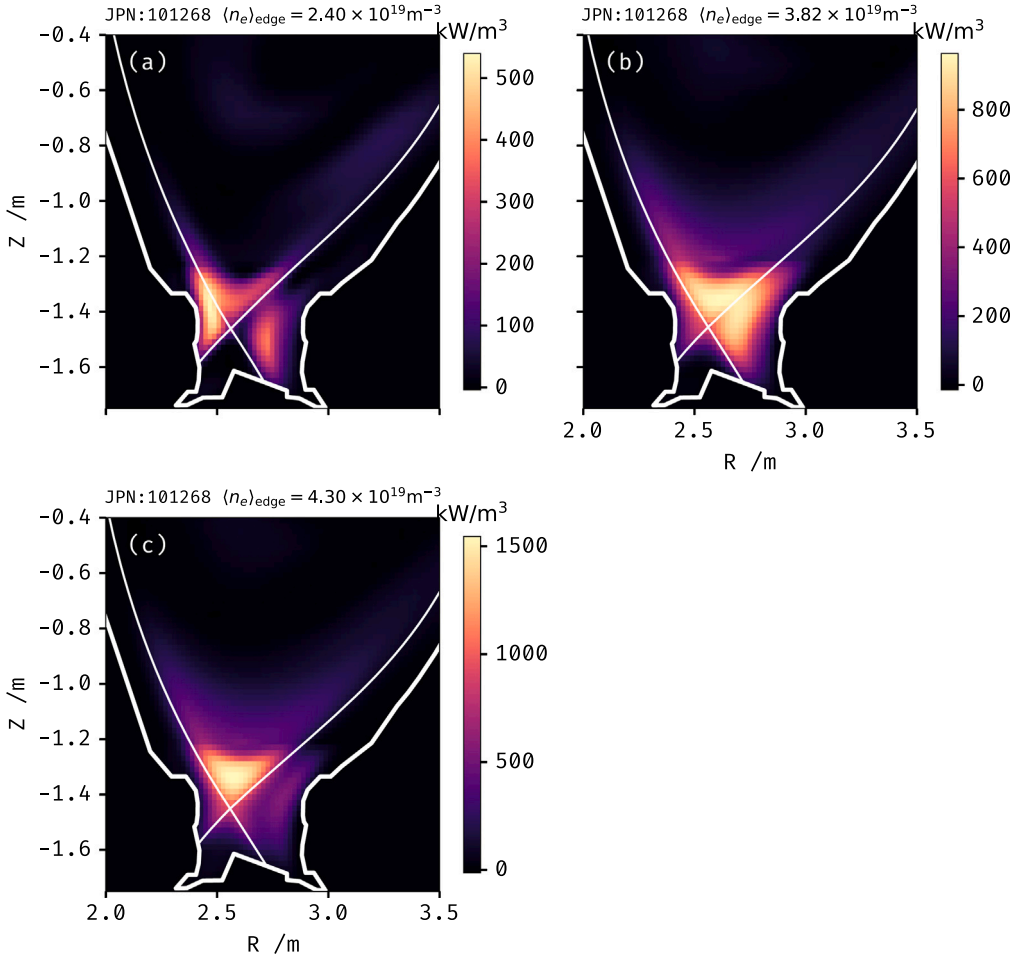

Fig. 6. Total radiated power density tomographic reconstructions from bolometry of $P_{NBI} = 5$ MW He plasma JPN 101268 for (a) $\langle n_e \rangle_{edge} = 2.4 \times 10^{19}$ m^{-3}, (b) $\langle n_e \rangle_{edge} = 3.8 \times 10^{19}$ m^{-3}, and (c) $\langle n_e \rangle_{edge} = 4.3 \times 10^{19}$ m^{-3}.

CRediT authorship contribution statement

D. Rees: Conceptualization, Formal analysis, Methodology, Software, Visualization, Writing – original draft. **M. Groth:** Conceptualization, Data curation, Funding acquisition, Investigation, Project administration, Resources, Supervision, Writing – review & editing, Methodology. **S. Aleiferis:** Data curation, Formal analysis, Investigation. **S. Brezinsek:** Conceptualization, Project administration, Funding acquisition. **M. Brix:** Data curation, Investigation, Validation. **I. Jepu:** Data curation, Investigation, Validation. **K.D. Lawson:** Data curation, Investigation, Validation. **A.G. Meigs:** Data curation, Investigation, Validation. **S. Menmuir:** Data curation, Investigation, Validation. **K. Kirov:** Investigation, Project administration. **P. Lomas:** Investigation. **C. Lowry:** Investigation, Project administration. **B. Thomas:** Data curation, Investigation, Validation. **A. Widdowson:** Data curation, Investigation, Project administration, Validation. **P. Carvalho:** Data curation, Investigation, Validation. **JET Contributors:** Data curation, Investigation, Validation.

Declaration of competing interest

The authors declare that they have no known competing financial interests or personal relationships that could have appeared to influence the work reported in this paper.

Data availability

Data will be made available on request.

Acknowledgements

This work has been carried out within the framework of the EUROfusion Consortium, funded by the European Union via the Euratom Research and Training Programme (Grant Agreement No 101052200 — EUROfusion). Views and opinions expressed are however those of the author(s) only and do not necessarily reflect those of the European Union or the European Commission. Neither the European Union nor the European Commission can be held responsible for them.

References

[1] ITER Organization, ITER Research Plan within the Staged Approach (Level III - Provisional Version), Tech. Rep. ITR-18-003, ITER Organization, France, 2018, p. 418, URL https://www.iter.org/technical-reports?id=9.

[2] R.A. Pitts, X. Bonnin, F. Escourbiac, H. Frerichs, J.P. Gunn, T. Hirai, A.S. Kukushkin, E. Kaveeva, M.A. Miller, D. Moulton, V. Rozhansky, I. Senichenkov, E. Sytova, O. Schmitz, P.C. Stangeby, G. De Temmerman, I. Veselova, S. Wiesen, Physics basis for the first ITER tungsten divertor, Nucl. Mater. Energy 20 (2019) 100696, http://dx.doi.org/10.1016/j.nme.2019.100696.

[3] F. Escourbiac, A. Durocher, A. Fedosov, T. Hirai, R.A. Pitts, P. Gavila, B. Riccardi, V. Kuznetcov, A. Volodin, A. Komarov, Assessment of critical heat flux margins on tungsten monoblocks of the ITER divertor vertical targets, Fusion Eng. Des. 146 (2019) 2036–2039, http://dx.doi.org/10.1016/j.fusengdes.2019.03.094.

[4] R.P. Wenninger, M. Bernert, T. Eich, E. Fable, G. Federici, A. Kallenbach, A. Loarte, C. Lowry, D. McDonald, R. Neu, T. Pütterich, P. Schneider, B. Sieglin, G. Strohmayer, F. Reimold, M. Wischmeier, DEMO divertor limitations during and in between ELMs, Nucl. Fusion 54 (11) (2014) 114003, http://dx.doi.org/10.1088/0029-5515/54/11/114003.

[5] M. Wischmeier, D. Coster, X. Bonnin, T. Eich, A. Huber, C. Ingesson, S. Jachmich, A. Kukushkin, A. Loarte, G.F. Matthews, R.A. Pitts, J. Rapp, D. Reiter, E. Tsitrone, Contributors EFDA-JET Work Programme, Divertor detachment during pure helium plasmas in JET, J. Nucl. Mater. 313–316 (2003) 980–985, http://dx.doi.org/10.1016/S0022-3115(02)01427-7.

[6] R.A. Pitts, P. Andrew, Y. Andrew, M. Becoulet, I. Coffey, D. Coster, D.C. McDonald, T. Eich, S.K. Erents, M.E. Fenstermacher, W. Fundamenski, G. Haas, A. Hermann, C. Hidalgo, D. Hillis, A. Huber, L.C. Ingesson, S. Jachmich, A. Kallenbach, A. Korotkov, K. Lawson, P. Lomas, T. Loarer, A. Loarte, G.F. Matthews, G. McCracken, A. Meigs, P. Mertens, M. O'Mullane, V. Philipps, G. Porter, A. Pospieszczyk, J. Rapp, D. Reiter, V. Riccardo, G. Saibene, R. Sartori, M.F. Stamp, E. Tsitrone, M. Wischmeier, J. Gafert, Contributors to the EFDA-JET workprogramme, Comparing scrape-off layer and divertor physics in JET pure He and D discharges, J. Nucl. Mater. 313–316 (2003) 777–786, http://dx.doi.org/10.1016/S0022-3115(02)01429-0.

[7] J.M. Canik, A.R. Briesemeister, A.G. McLean, M. Groth, A.W. Leonard, J.D. Lore, A. Moser, BPMIC Team, Testing the role of molecular physics in dissipative divertor operations through helium plasmas at DIII-D, Phys. Plasmas 24 (5) (2017) 056116, http://dx.doi.org/10.1063/1.4982057.

[8] J. Liu, L. Meng, H. Guo, K. Li, J. Xu, H. Wang, G. Xu, F. Ding, L. Zhang, Y. Duan, B. Zhang, L. Yu, P. Wang, A. Li, D. Wu, R. Ding, L. Wang, Divertor detachment operation in helium plasmas with ITER-like tungsten divertor in EAST, Plasma Sci. Technol. 24 (7) (2022) 075101, http://dx.doi.org/10.1088/2058-6272/ac621d.

[9] G.F. Matthews, M. Beurskens, S. Brezinsek, M. Groth, E. Joffrin, A. Loving, M. Kear, M.-L. Mayoral, R. Neu, P. Prior, V. Riccardo, F. Rimini, M. Rubel, G. Sips, E. Villedieu, P. de Vries, M.L. Watkins, EFDA-JET contributors, JET ITER-like wall—overview and experimental programme, Phys. Scr. 2011 (T145) (2011) 014001, http://dx.doi.org/10.1088/0031-8949/2011/T145/014001.

[10] N. Horsten, M. Groth, W. Dekeyser, W. Van Uytven, S. Aleiferis, S. Carli, J. Karhunen, K.D. Lawson, B. Lomanowski, A.G. Meigs, S. Menmuir, A. Shaw, V. Solokha, B. Thomas, Validation of SOLPS-ITER simulations with kinetic, fluid, and hybrid neutral models for JET-ILW low-confinement mode plasmas, Nucl. Mater. Energy 33 (2022) 101247, http://dx.doi.org/10.1016/j.nme.2022.101247.

[11] M. Groth, S. Brezinsek, P. Belo, G. Corrigan, D. Harting, S. Wiesen, M.N.A. Beurskens, M. Brix, M. Clever, J.W. Coenen, T. Eich, J. Flanagan, C. Giroud, A. Huber, S. Jachmich, U. Kruezi, M. Lehnen, C. Lowry, C.F. Maggi, S. Marsen, A.G. Meigs, G. Sergienko, B. Sieglin, C. Silva, A. Sirinelli, M.F. Stamp, G.J. van Rooij, Target particle and heat loads in low-triangularity L-mode plasmas in JET with carbon and beryllium/tungsten walls, J. Nucl. Mater. 438 (2013) S175–S179, http://dx.doi.org/10.1016/j.jnucmat.2013.01.072.

[12] K. Verhaegh, A.C. Williams, D. Moulton, B. Lipschultz, B.P. Duval, O. Février, A. Fil, J. Harrison, N. Osborne, H. Reimerdes, C. Theiler, t.T. Team, t.E.M. Team, Investigating the impact of the molecular charge-exchange rate on detached SOLPS-ITER simulations, Nucl. Fusion 63 (7) (2023) 076015, http://dx.doi.org/10.1088/1741-4326/acd394.

[13] M. Groth, S. Brezinsek, P. Belo, M.N.A. Beurskens, M. Brix, M. Clever, J.W. Coenen, C. Corrigan, T. Eich, J. Flanagan, C. Guillemaut, C. Giroud, D. Harting, A. Huber, S. Jachmich, U. Kruezi, K.D. Lawson, M. Lehnen, C. Lowry, C.F. Maggi, S. Marsen, A.G. Meigs, R.A. Pitts, G. Sergienko, B. Sieglin, C. Silva, A. Sirinelli, M.F. Stamp, G.J. van Rooij, S. Wiesen, the JET-EFDA Contributors, Impact of carbon and tungsten as divertor materials on the scrape-off layer conditions in JET, Nucl. Fusion 53 (9) (2013) 093016, http://dx.doi.org/10.1088/0029-5515/53/9/093016.

[14] E.R. Solano, E. Delabie, G. Birkenmeier, C. Silva, J.C. Hillesheim, P. Vincenzi, A.H. Nielsen, J.J. Rasmussen, A. Baciero, S. Aleiferis, I. Balboa, A. Boboc, C. Bourdelle, I.S. Carvalho, P. Carvalho, M. Chernyshova, R. Coelho, T. Craciunescu, R. Dumont, P. Dumortier, E. de la Luna, J. Flanagan, M. Fontana, J.M. Fontdecaba, L. Frassinetti, D. Gallart, J. Garcia, E. Giovannozzi, C. Giroud, W. Gromelski, R. Henriques, L. Horvath, P. Jacquet, I. Jepu, A. Kappatou, D.L. Keeling, D. King, E. Kowalska-Strzęciwilk, M. Lennholm, E. Lerche, E. Litherland-Smith, V. Kiptily, K. Kirov, A. Loarte, B. Lomanowski, C.F. Maggi, M.J. Mantsinen, A. Manzanares, M. Maslov, A.G. Meigs, I. Monakhov, R.B. Morales, D. Nina, C. Noble, V. Parail, F.P. Diaz, E. Pawelec, G. Pucella, D. Réfy, E. Righi-Steele, F.G. Rimini, T. Robinson, S. Saarelma, M. Sertoli, A. Shaw, S. Silburn, P. Sirén, Ž. Štancar, H. Sun, G. Szepesi, D. Taylor, E. Tholerus, S. Vartanian, G. Verdoolaege, B. Viola, H. Weisen, T. Wilson, J.E.T. Contributors, Recent progress in L–H transition studies at JET: Tritium, helium, hydrogen and deuterium, Nucl. Fusion 62 (7) (2022) 076026, http://dx.doi.org/10.1088/1741-4326/ac4ed8.

[15] S. Vartanian, E. Delabie, C.C. Klepper, I. Jepu, P. Jacquet, E. Lerche, B. Lomanowski, L. Colas, C. Marcus, R. Dumond, D. Douai, A. Widdowson, Simultaneous H/D/T and 3He/4He absolute concentration measurements with an optical penning gauge on JET, Fusion Eng. Des. 170 (2021) 112511, http://dx.doi.org/10.1016/j.fusengdes.2021.112511.

[16] M. Groth, S. Brezinsek, P. Belo, M. Brix, G. Calabro, A. Chankin, M. Clever, J.W. Coenen, G. Corrigan, P. Drewelow, C. Guillemaut, D. Harting, A. Huber, S. Jachmich, A. Järvinen, U. Kruezi, K.D. Lawson, M. Lehnen, C.F. Maggi, C. Marchetto, S. Marsen, F. Maviglia, A.G. Meigs, D. Moulton, C. Silva, M.F. Stamp, S. Wiesen, Divertor plasma conditions and neutral dynamics in horizontal and vertical divertor configurations in JET-ILW low confinement mode plasmas, J. Nucl. Mater. 463 (2015) 471–476, http://dx.doi.org/10.1016/j.jnucmat.2014.12.030.

[17] J. Karhunen, B. Lomanowski, V. Solokha, S. Aleiferis, P. Carvalho, M. Groth, K.D. Lawson, A.G. Meigs, A. Shaw, J.E.T. Contributors, Assessment of filtered cameras for quantitative 2D analysis of divertor conditions during detachment in JET L-mode plasmas, Plasma Phys. Control. Fusion 63 (8) (2021) 085018, http://dx.doi.org/10.1088/1361-6587/ac0b9e.

[18] V. Solokha, M. Groth, G. Corrigan, S. Wiesen, Interpretation of the hydrogen isotope effect on the density limit in JET-ILW L-mode plasmas using EDGE2d-EIRENE, Phys. Scr. 96 (12) (2021) 124028, http://dx.doi.org/10.1088/1402-4896/ac267c.

[19] M. Groth, V. Solokha, S. Aleiferis, S. Brezinsek, M. Brix, I.S. Carvalho, P. Carvalho, G. Corrigan, D. Harting, N. Horsten, I. Jepu, J. Karhunen, K. Kirov, B. Lomanowski, K.D. Lawson, C. Lowry, A.G. Meigs, S. Menmuir, E. Pawelec, T. Pereira, A. Shaw, S. Silburn, B. Thomas, S. Wiesen, P. Börner, D. Borodin, S. Jachmich, D. Reiter, G. Sergienko, Z. Stancar, B. Viola, P. Beaumont, J. Bernardo, I. Coffey, N.J. Conway, E. de la Luna, D. Douai, C. Giroud, J. Hillesheim, L. Horvath, A. Huber, P. Lomas, C.F. Maggi, M. Maslov, C. Perez von Thun, S. Scully, N. Vianello, M. Wischmeier, Characterisation of divertor detachment onset in JET-ILW hydrogen, deuterium, tritium and deuterium–tritium low-confinement mode plasmas, Nucl. Mater. Energy 34 (2023) 101345, http://dx.doi.org/10.1016/j.nme.2022.101345.

[20] H.A. Kumpulainen, M. Groth, G. Corrigan, D. Harting, F. Koechl, A.E. Jaervinen, B. Lomanowski, A.G. Meigs, M. Sertoli, Validation of EDGE2d-EIRENE and DIVIMP for W SOL transport in JET, Nucl. Mater. Energy 25 (2020) 100866, http://dx.doi.org/10.1016/j.nme.2020.100866.

[21] K.-D. Zastrow, S.J. Cox, M.G. von Hellermann, M.G. O'Mullane, D. Stork, M. Brix, C.D. Challis, I.H. Coffey, R. Dux, K.H. Finken, C. Giroud, D. Hillis, J.T. Hogan, K.D. Lawson, T. Loarer, A.G. Meigs, P.D. Morgan, M.F. Stamp, A.D. Whiteford, JET EFDA Contributors, Helium exhaust experiments on JET with type I ELMs in h-mode and with type III elms in ITB discharges, Nucl. Fusion 45 (3) (2005) 163, http://dx.doi.org/10.1088/0029-5515/45/3/002.

[22] U. Kruezi, G. Sergienko, P.D. Morgan, G.F. Matthews, S. Brezinsek, S. Vartanian, JET-EFDA Contributors, JET divertor diagnostic upgrade for neutral gas analysis, Rev. Sci. Instrum. 83 (10) (2012) 10D728, http://dx.doi.org/10.1063/1.4732175.

[23] U. Kruezi, I. Jepu, G. Sergienko, C.C. Klepper, E. Delabie, S. Vartanian, A. Widdowson, Neutral gas analysis for JET DT operation, J. Instrum. 15 (01) (2020) C01032, http://dx.doi.org/10.1088/1748-0221/15/01/C01032.

[24] A. Huber, K. McCormick, P. Andrew, P. Beaumont, S. Dalley, J. Fink, J.C. Fuchs, K. Fullard, W. Fundamenski, L.C. Ingesson, F. Mast, S. Jachmich, G.F. Matthews, P. Mertens, V. Philipps, R.A. Pitts, S. Sanders, W. Zeidner, Upgraded bolometer system on JET for improved radiation measurements, Fusion Eng. Des. 82 (5) (2007) 1327–1334, http://dx.doi.org/10.1016/j.fusengdes.2007.03.027.

[25] A. Boboc, C. Gil, P. Pastor, P. Spuig, T. Edlington, S. Dorling, JET-EFDA Contributors, Upgrade of the JET far infrared interferometer diagnostic, Rev. Sci. Instrum. 83 (10) (2012) 10E341, http://dx.doi.org/10.1063/1.4737420.

[26] GPy, GPy: a Gaussian processes framework in python, 2023, URL https://github.com/SheffieldML/GPy. Sheffield Machine Learning Software.

[27] A.W. Leonard, Plasma detachment in divertor tokamaks, Plasma Phys. Control. Fusion 60 (4) (2018) 044001, http://dx.doi.org/10.1088/1361-6587/aaa7a9.

[28] P.C. Stangeby, The Plasma Boundary of Magnetic Fusion Devices, in: Plasma Physics Series, IOP Publishing, Bristol ; Philadelphia, 2000, URL https://doi.org/10.1201/9780367801489.

[29] V. Solokha, M. Groth, S. Brezinsek, M. Brix, G. Corrigan, C. Guillemaut, D. Harting, S. Jachmich, U. Kruezi, S. Marsen, S. Wiesen, The role of drifts on the isotope effect on divertor plasma detachment in JET ohmic discharges, Nucl. Mater. Energy 25 (2020) 100836, http://dx.doi.org/10.1016/j.nme.2020.100836.

[30] B. Lomanowski, M. Carr, A. Field, M. Groth, A.E. Jaervinen, C. Lowry, A.G. Meigs, S. Menmuir, M. O'Mullane, M.L. Reinke, C.K. Stavrou, S. Wiesen, Spectroscopic investigation of N and Ne seeded induced detachment in JET ITER-like wall l-modes combining experiment and EDGE2d modeling, Nucl. Mater. Energy 20 (2019) 100676, http://dx.doi.org/10.1016/j.nme.2019.100676.

[31] S.I. Krasheninnikov, A.S. Kukushkin, A.A. Pshenov, Divertor plasma detachment, Phys. Plasmas 23 (5) (2016) 055602, http://dx.doi.org/10.1063/1.4948273.

[32] D. Reiter, The data file AMJUEL: additional atomic and molecular data for EIRENE, 2020.

[33] P.C. Stangeby, A problem in the interpretation of tokamak langmuir probes when a fast electron component is present, Plasma Phys. Control. Fusion 37 (9) (1995) 1031, http://dx.doi.org/10.1088/0741-3335/37/9/008.

[34] J. Horacek, R.A. Pitts, P.C. Stangeby, O. Batishchev, A. Loarte, Predicted effects of parallel temperature gradients on the overestimation of TCV divertor target langmuir probe Te measurements, J. Nucl. Mater. 313–316 (2003) 931–935, http://dx.doi.org/10.1016/S0022-3115(02)01479-4.

[35] F. Militello, Boundary Plasma Physics: An Accessible Guide to Transport, Detachment, and Divertor Design, in: Springer Series on Atomic, Optical, and Plasma Physics, vol. 123, Springer International Publishing, Cham, 2022, http://dx.doi.org/10.1007/978-3-031-17339-4.

[36] K. Verhaegh, B. Lipschultz, J.R. Harrison, B.P. Duval, A. Fil, M. Wensing, C. Bowman, D.S. Gahle, A. Kukushkin, D. Moulton, A. Perek, A. Pshenov, F. Federici, O. Février, O. Myatra, A. Smolders, C. Theiler, t.T. Team, t.E.M. Team, The role of plasma-molecule interactions on power and particle balance during detachment on the TCV tokamak, Nucl. Fusion 61 (10) (2021) 106014, http://dx.doi.org/10.1088/1741-4326/ac1dc5.